ELSEVIER

Chemistry and Physics of Lipids 73 (1994) 39–56

Chemistry and Physics of LIPIDS

Hidden dynamics in rapid changes of bilayer shape

E. Evans*, A. Yeung

Departments of Physics and Pathology, University of British Columbia, Vancouver, British Columbia V6T 1W5, Canada

Abstract

In the past, mechanical models for lipid bilayers have been conceptualized on the basis that the membrane is a 'unit' structure where energy is coupled to deformation through single fields for surface curvature and density — valid only for chemically bonded layers. By comparison, real bilayers are composed of two weakly adherent monolayers that can move slowly past one another with negligible input of local energy if shape remains constant. However, when bilayer shape changes rapidly, an unexpected viscous impedance arises from relative motion between layers, which significantly augments conventional retardation by dissipation in hydrodynamic flow. The added dissipation is produced by drag at the monolayer-monolayer interface. This leads to 'hidden dynamic coupling' of the layers through density differences that spread diffusively over the surface with long range consequences. Here, we examine the origins of mechanical coupling between layers in bilayers and show that evolution of the differential density between layers creates new dynamics previously overlooked in membrane behavior. To demonstrate the profound affect of dynamic coupling in bilayers, we describe a model situation (supported by experimental evidence) where a nanoscale tube of membrane is pulled rapidly from a macroscopic-size vesicle. Rapid extraction of bilayer through this 1000-fold increase in curvature creates an enormous relative motion between layers near the vesicle-tube junction (molecules in opposite layers slip past at rates approaching 10^5/s) and, in turn, interlayer drag that dominates the extraction force.

Keywords: Bilayer mechanics; Vesicle shape dynamics; Stratified membranes; Interlayer coupling and dissipation; Vesicle bilayer tethers

1. Introduction

Surfactant bilayers represent an important class of self-assembled structures with a rich set of phases and complex transitions [1,2]. The molecularly-thin structure is exceptionally flexible; therefore, bilayer capsules or vesicles are easily deformed into shapes with bizarre highly-curved contours and even weak thermal fluctuations can roughen the surface significantly. This unusual 'softness' and other exotic features of bilayers have stimulated many theoretical developments over the past twenty years beginning with simple elastic models [3,4] and shape predictions [5,6], followed by thermodynamic and dynamic analyses of fluctuations [7,8], studies of adhesion [9,10] and unbinding transitions [11,12], and — most recently — models for spontaneous shape changes in vesicles [13,14]. Almost all of these theoretical developments have been conceptualized on the basis of mechanical behavior for a 'unit' membrane structure, i.e., as if the monolayers of the bilayer were chemically bonded together at the midplane. The Hamiltonians proposed for collective excitations have coupled energy to deformation through fields for surface density and curvature. As such, material properties have been char-

* Corresponding author, Tel.: 604 8227103.

SSDI 0009-3084(94)02358-C

acterized by 'unit' elastic moduli for area compressibility and bending rigidity plus surface viscosity — again appropriate for single layers or bonded strata. However, the situation is clearly different for surfactant bilayers; the monolayers are drawn together by only weak van der Waals attraction emanating from the aqueous half spaces surrounding the bilayer. At equilibrium, the monolayers of the bilayer can easily slide relative to one another with no change in energy provided that the surface shape remains fixed. Therefore, bending a bilayer seems to merely involve curving two adjacent monolayers to follow a common form with little interaction between layers. On the other hand, rapid displacements between layers are expected to be opposed by viscous drag at the bilayer midplane, which will lead to 'dynamic coupling' of the layers causing them to behave as if connected. Consequently, changes in shape of bilayer capsules that create relative motion between monolayers (e.g., large changes in curvature) involve a hidden dynamic impedance superposed on the hydrodynamic resistance of the aqueous environment. As we have shown [15,16], dissipation in bilayer membranes is highly nonlocal and intervenes on lengths close to macroscopic to overtake conventional hydrodynamic losses. Indeed, rapid changes in curvature throughout the mesoscopic scale are expected to be retarded almost entirely by the viscous coupling between monolayers. For capsules with closed-spherical topology, another global consequence of bilayer structure is nonlocal curvature elasticity that plays a role analogous to spontaneous curvature in shape determination [4,14,17]. The origin of these subtle features lies in the coupling of forces between layers of a stratified membrane.

Examining the mechanical forces in a bilayer, we will demonstrate that relative motion (slip) between layers is driven by differences of the tension fields supported by the monolayers. The tension differences produce local-diffential dilations (density differences) between layers that define a new field on the surface. Evolution of the differential dilation field leads to new dynamics here-to-fore neglected in membrane behavior. We will illustrate the special dynamic consequences of this field with an analysis of steady extraction of a bilayer tether (submicroscopic tube ~ 10 nm radius) from a macroscopic-size vesicle. Here, the membrane is made to flow rapidly through a 1000-fold increase in curvature. We will show that the dynamic force required to pull a tube from a vesicle surface is totally dominated by intermonolayer drag — conventional hydrodynamic resistance is negligible. (Throughout the following developments, there is a significant amount of unavoidable formulism. We have reduced this to a parsimonious set of relations that encompass the important consequences of intermonolayer coupling in bilayers with references given to details published elsewhere.)

2. Stratified membranes as equivalent mechanical surfaces

2.1. Surface force fields

A thin material can be represented by an equivalent mechanical surface of zero thickness through cumulation of forces (stresses) over its cross section — provided that the thickness h is much smaller than the radii of curvature characterizing the contours of the surface shape [17]. The outcome is a set of force resultants — lateral tensions that act tangent to the plane of the surface and transverse shears that act to 'cut' the surface — plus surface tractions applied by external forces. Specializing to situations of axial symmetry, the surface curvatures and force resultants reduce to the diagonal representations illustrated schematically in Fig. 1A. The principal curvatures c_m, c_ϕ are functions of the polar angle θ formed between the local surface normal and the axis of symmetry as given by,

$$c_m = \frac{\partial \theta}{\partial s} \qquad c_\phi = \frac{\sin\theta}{r}$$
$$\bar{c} \equiv c_m + c_\phi = \frac{1}{r}\,\frac{\partial}{\partial r}\,(r \cdot \sin\theta) \tag{1}$$

where s is the longitudinal (curvilinear) distance along the meridian and r is the circular radius measured from the symmetry axis z. The surface tensions include a meridional component τ_m along contours and a circumferential component τ_ϕ

tangent to latitude circles. However, because of cylindrical symmetry, only a single transverse shear component Q_m survives which acts normal to the surface along latitude circles as shown. External forces lead to a normal traction (outward pressure) P_n and a shear traction P_t tangent to the meridian. Clearly, lateral tensions and transverse shear are forces distributed per length along contours and circles embedded in the equivalent surface whereas external tractions are forces distributed per area of the surface. Differential balances of forces supported by the equivalent surface element yield two local conditions of mechanical equilibrium as follows [17]: first, in the direction normal to the surface, a generalized 'law of Laplace' is obtained where tensions scaled by curvatures plus divergence of the transverse shear balance the normal traction (pressure P_n),

$$P_n = \tau_m c_m + \tau_\phi c_\phi - \frac{1}{r}\frac{\partial}{\partial s}(r \cdot Q_m) \tag{2}$$

Second, tangent to the surface, the shear traction P_t is balanced by divergence of lateral tensions plus a small lateral projection of transverse shear due to curvature,

$$-P_t = \frac{1}{r}\frac{\partial}{\partial s}(r \cdot \tau_m) - \frac{\tau_\phi}{r}\frac{\partial r}{\partial s} + c_m Q_m \tag{3}$$

Although the force resultants and tractions sketched in Fig. 1A establish local force equilibrium for the thin material (assuming inertial and body forces are negligible), the subtle feature is that local torques are not balanced at this stage. Normally, symmetry of the stress field (tensor) ensures that torques about the element centroid are balanced; but collapse of the material to an equivalent surface 'breaks' this symmetry so that other fields are needed. To ensure that torques are balanced, surface moment resultants M_m and M_ϕ illustrated in Fig. 1B must be included. Divergence of surface moments offsets the torque about the element center produced by the transverse shear Q_m as given by;

$$Q_m = \frac{1}{r}\frac{\partial}{\partial s}(r \cdot M_m) - \frac{M_\phi}{r}\frac{\partial r}{\partial s} \tag{4}$$

Thus, divergence of the moment fields replaces the contribution of transverse shear Q_m in Eqs.

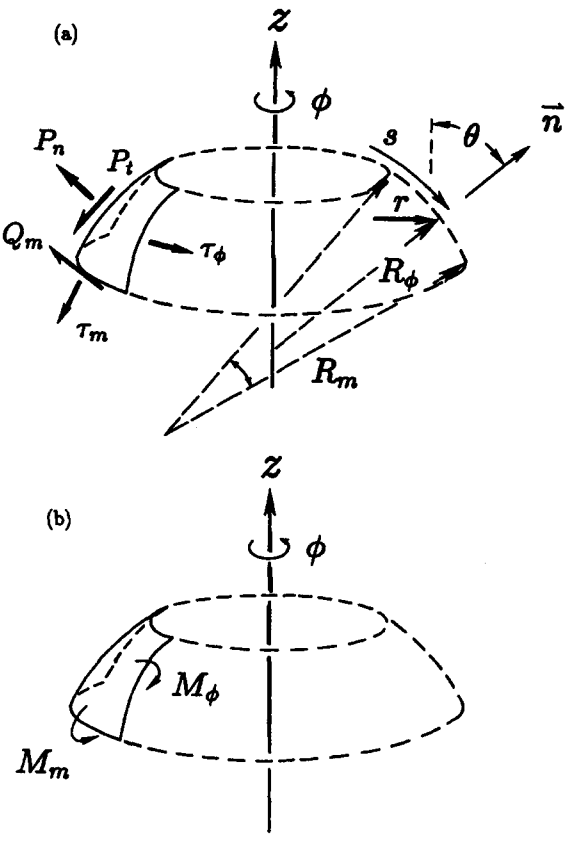

Fig. 1. (A) Schematic diagram of an element of the equivalent mechanical surface used to represent an axisymmetric membrane capsule. Cumulation of stresses in the membrane leads to lateral tensions τ_m, τ_ϕ and a transverse shear force Q_m distributed along contours as shown. External forces reduce to normal and tangential surface tractions P_n, P_t. Principal curvatures $1/R_m$, $1/R_\phi$ and intrinsic curvilinear coordinates s, θ describe the geometry of the axially symmetric shape. (B) Illustration of the moment fields required to ensure local balance of torques about the element centroid.

(2) and (3). A useful corollary to local force balances is zero-net force along the symmetry axis, i.e.,

$$0 = -\int_1^2 (P_n \cdot \cos\theta - P_t \cdot \sin\theta) r \cdot ds + [r \cdot \tau_m \cdot \sin\theta - r \cdot Q_m \cdot \cos\theta]_1^2 \tag{5}$$

which is found directly by integration of Eqs. (2) and (3), multiplied by cos θ and sin θ, respectively, between sections perpendicular to the axis of symmetry. Consequently, any choice of two

relations from Eqs (2), (3) and (5) can be used to specify mechanical force equilibrium in the surface. (*Note:* because of the small dimension scale (a few μm) typical for membrane capsules, inertial forces and acceleration can almost always be neglected.)

2.2. Continuum stress fields

From a continuum perspective, the task is to relate the lateral tension and moment fields to integrals of stresses within the material. Conceptually [16,17], this simply involves cumulation of lateral forces and moments of these forces over the various strata of the material as related to the location of the equivalent surface — commonly referred to as the 'neutral surface'. As sketched in Fig. 2, lateral stresses σ_m, σ_ϕ create forces per length along arcs tangent to latitude circles and meridians, which are scaled by the thickness d_x of a stratum and are augmented by excess dimensions $x \cdot c_\phi$, $x \cdot c_m$ of the stratum relative to equivalent surface dimensions (separated by a distance x). In addition, these lateral forces contribute moments to the equivalent surface in proportion

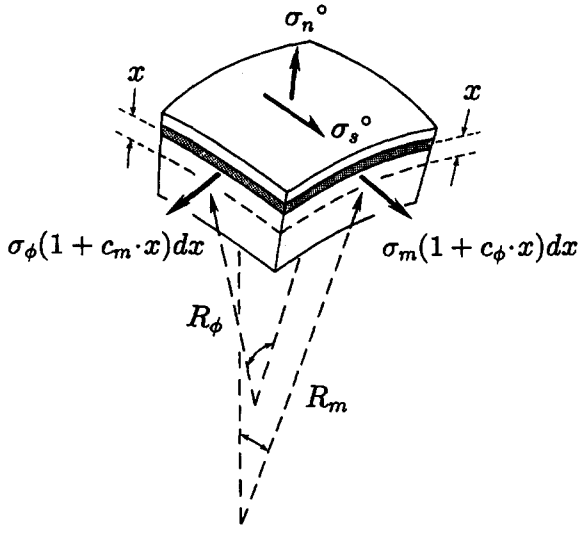

Fig. 2. Schematic of force resultants projected onto the equivalent surface by lateral stresses distributed continuously within the membrane.

to the separation distance. Hence, for continuous material stresses, representation of the membrane as an equivalent mechanical surface follows directly by integrating these differential force contributions over the membrane thickness [16]. The result defines generalized tension and moment fields embedded in the surface:

$$\tau_m \equiv \mathring{\tau}_m + c_\phi M_m \qquad \tau_\phi \equiv \mathring{\tau}_\phi + c_m M_\phi$$

$$\mathring{\tau}_m \equiv \int \sigma_m \cdot dx \qquad \mathring{\tau}_\phi \equiv \int \sigma_\phi \cdot dx \qquad (6)$$

$$M_m \approx \int (x \cdot \sigma_m) dx \qquad M_\phi \approx \int (x \cdot \sigma_\phi) dx$$

(*Note:* second moments of stress have been neglected since they are extremely small. If needed, the higher order terms can readily be included.) It is important that the location of the equivalent surface within the material strata be defined to ensure that moments in Eq. (6) are unique definitions. In general, definition of the neutral surface can be nontrivial or even impossible. Usually for homogeneous-linear materials, the convention is to choose the midplane of the membrane (the so-called Kirchoff hypothesis). For discrete multilayered fluids, precise definition can be found from moments of the layer elastic moduli [17]. Here, we avoid these technical issues and merely assume that a suitable definition exists. From Eq. (6), we see that the generalized tension fields, which live on the equivalent surface, include contributions from both zero moments of lateral stresses (*planar* tensions $\mathring{\tau}_m$, $\mathring{\tau}_\phi$) and the first moments of stresses (M_m,M_ϕ). Using these field components, the force balances for the equivalent surface can be expressed in a form that is related directly to planar mechanical properties of the membrane strata (see Appendix A). In turn, constitutive (elastic and viscous) specifications for layer stresses in terms of planar deformations (dilatation and shear) relate these tensions and moments to the kinematics of surface motion. When combined with the equilibrium balances (Eqs. (2), (3) or (5)), a complete description is obtained for the dynamics of a chemically-bonded membrane under the action of external forces.

2.3. Interlayer coupling fields

Uncoupled or weakly-adherent membrane strata require additional equations of motion to specify relative displacements between layers. In particular, interlayer shear stresses $\sigma_s(l)^{\pm}$ must be introduced into the balance of lateral forces for each layer (denoted by 'l'); these tractions are imparted to a layer by adjacent strata (above and below,). Using the planar tensions $\mathring{\tau}_m(l)$, $\mathring{\tau}_\phi(l)$ and moments $M_m(l)$, $M_\phi(l)$ defined for a layer by integrals of lateral stresses (Eq. 6), the balance of lateral forces on each layer is expressed by,

$$
\begin{aligned}
&-\Delta\sigma_s(l)(1+\bar{x}_l\cdot\bar{c}) \\
&\quad=\left\{\frac{1}{r}\,\frac{\partial}{\partial s}[r\cdot\mathring{\tau}_m(l)]-\frac{\mathring{\tau}_\phi(l)}{r}\,\frac{\partial r}{\partial s}\right\} \\
&\qquad+\bar{c}\left\{\frac{1}{r}\,\frac{\partial}{\partial s}[r\cdot M'_m(l)]-\frac{M'_\phi(l)}{r}\,\frac{\partial r}{\partial s}\right\} \\
&\qquad+\left[M'_m(l)-M'_\phi(l)\right]\frac{\partial c_\phi}{\partial s}
\end{aligned}
\tag{7}
$$

$$
\begin{aligned}
&-\Delta\sigma_s(l)(1+\bar{x}_l\cdot\bar{c})\equiv-\sigma_s^+(l)(1+x_l^+\cdot\bar{c}) \\
&\quad+\sigma_s^-(l)(1+x_l^-\cdot\bar{c}) \\
&\sigma_s^-(l+1)\equiv\sigma_s^+(l)\qquad\sigma_s^+(l-1)\equiv\sigma_s^-(l)
\end{aligned}
$$

where couples of planar tensions (scaled by the position $\bar{x}_l$ relative to the location of the equivalent surface) add to the intrinsic moments of stress within each layer,

$$
\begin{aligned}
M'_m(l)&\equiv M_m(l)+\bar{x}_l\cdot\mathring{\tau}_m(l) \\
M'_\phi(l)&\equiv M_\phi(l)+\bar{x}_l\cdot\mathring{\tau}_\phi(l)
\end{aligned}
$$

Interlayer stresses act oppositely on the upper/lower surfaces of the layers that form an interface; therefore, they disappear from the force balances when cumulated over all membrane strata leaving the total tractions P_n, P_t (defined in Appendix B). Hence, cumulation of forces for an unbonded membrane preserves the local balances given in Eqs. (2–5) where tension and moment fields become sums over layer contributions but important contributions arise from couples of layer tensions. Even though interlayer shear stresses do not appear explicitly in these totals, they regulate variations in lateral force resultants amongst layers which, in turn, drive relative displacements between the layers. Mechanically, the layers interact through the moment fields. Using Eq. (7), deviations of lateral forces between membrane strata can be written explicitly for multilayer interfaces but notation is cumbersome and provides little reduction in complexity. Since our focus is bilayers, we will specialize the remainder of the analysis to two layer structures.

For simplicity, we assume that the interface between layers of a bilayer defines the location of the equivalent mechanical surface and that the positions of action for the planar tensions in each layer lie at the same distance from the interface (given by $\pm h/a$ where $a \geq 2$). Given this abstraction of bilayer structure, the total tension and moment fields required in the local balances of force are defined by,

$$
\begin{aligned}
&\mathring{\tau}_m\equiv\mathring{\tau}_m(2)+\mathring{\tau}_m(1)\qquad\mathring{\tau}_\phi\equiv\mathring{\tau}_\sigma(2)+\mathring{\tau}_\phi(1) \\
&\Delta\mathring{\tau}_m\equiv\mathring{\tau}_m(2)-\mathring{\tau}_m(1)\qquad\Delta\mathring{\tau}_\phi\equiv\mathring{\tau}_\phi(2)-\mathring{\tau}_\phi(1) \\
&M'_m\equiv M_m(2)+M_m(1)+\tfrac{h}{a}\cdot\Delta\mathring{\tau}_m \\
&M'_\phi\equiv M_\phi(2)+M_\phi(1)+\tfrac{h}{a}\cdot\Delta\mathring{\tau}_\phi
\end{aligned}
\tag{8}
$$

Next, Eq. (7) is used to specify a balance of lateral forces in each layer. Then, the difference between these balances is taken to isolate the interlayer coupling stress. Eliminating terms of second order as described in Appendix C, it follows that deviation in lateral tensions $\Delta\mathring{\tau}_m$, $\Delta\mathring{\tau}_\phi$ between layers is driven by shear stress σ_s (drag) at the monolayer-monolayer interface:

$$
2\bar{\sigma}_s=\frac{1}{r}\,\frac{\partial}{\partial s}(r\cdot\Delta\mathring{\tau}_m)-\frac{\Delta\mathring{\tau}_\phi}{r}\cdot\frac{\partial r}{\partial s} \tag{9}
$$

When the constitutive relation for interlayer stress is introduced, Eq. (9) establishes the additional equation of motion needed to specify relative displacement between layers of an unbonded structure.

3. Fluid bilayers: statics

Above the melting temperature for lipid hydrocarbon chains, monolayers of a bilayer are con-

densed surface fluids [18,19]. For diacyl lipids with chain lengths greater than 12 carbons (dilauroyl, dimyristoyl, etc.), the constituents remain confined to the monolayers over time scales of laboratory experiments with no indication of transfer to the adjacent aqueous media. This apparent 'insolubility' defines a cohesive physical state where, at static equilibrium (no bilayer flow), lateral tension depends only on reduction in surface density (dilation $\alpha = \tilde{A}/\tilde{A}_o - 1$ in area per molecule $\tilde{A}$) relative to a reference density ρ_o ($= 1/\tilde{A}_o$) at zero tension, i.e.,

$$\mathring{\tau}_m(l) = \mathring{\tau}_\phi(l) = K \cdot \alpha(l) \equiv \mathring{\tau}(l)$$

The elastic proportionality is characterized by a modulus K for area compressibility. Likewise for curved monolayers, moments of chain stresses are 'isotropic' ($M_m = M_\phi$) and modeled by H another elastic proportionality,

$$M_m(l) = M_\phi(l) = k_c\,[\bar{c} - c_o(l)] \equiv M(l)$$

The modulus k_c represents bending stiffness and the reference curvature $c_o(l)$ is defined by surface contours where moments of stress in each monolayer are zero. Using these elastic relations in Eq. (8), we establish tension and moment fields for a bilayer surface at static equilibrium, i.e.,

$$\begin{aligned} \mathring{\tau} &= K\,[\alpha(2) + \alpha(1)] \equiv 2K \cdot \bar{\alpha} \\ \Delta\mathring{\tau} &= K[\alpha(2) - \alpha(1)] \equiv K \cdot \alpha_\pm \\ M &= 2k_c \cdot \bar{c} + \frac{h}{a} \cdot \Delta\mathring{\tau} \equiv 2k_c \cdot \bar{c} + M_\pm \end{aligned} \tag{10}$$

Locally, the mean dilation of the bilayer is expressed by $\bar{\alpha} = [\alpha(2) + \alpha(1)]/2$ and the differential dilation between layers is $\alpha_\pm = \alpha(2) - \alpha(1)$. In symmetric bilayers, the reference ('spontaneous') curvatures $c_o(1)$, $c_o(2)$ for bending the monolayers are opposite in sign and cancel out of the total bilayer moment. Furthermore, the moment contributed by the tension couple ($M_\pm = h\Delta\,\mathring{\tau}/a$) defines another modulus that can be arranged to appear as a bending elasticity $\bar{k}_c = h^2K/a^2$, i.e., $M_\pm = a\,\bar{k}_c\,\alpha_\pm/h$. (*Note:* the product of elastic area modulus K and thickness squared h^2 exposes the major determinants of bending rigidity in membranes. Thus, as experiments show [20], compositional variations that alter compressibility modify flexibility similarly.) The tension and moment relations given in Eq. (10) can now be used with Eqs. (2), (3) or (5) and (9) to establish the equilibrium shape of a bilayer under the action of external tractions P_n, P_t, i.e.,

$$P_n = \bar{\tau} \cdot \bar{c} - k_c\bar{c}(c_m - c_\phi)^2 + 2M_\pm c_m\, c_\phi - \frac{1}{r}\,\frac{\partial}{\partial s}\left[r \cdot \left(2k_c\frac{\partial \bar{c}}{\partial s} + \frac{\partial M_\pm}{\partial s}\right)\right] \tag{11}$$

$$\bar{\tau} \equiv \mathring{\tau} + k_c\bar{c}^2$$

$$-P_t = \frac{\partial \bar{\tau}}{\partial s} - \bar{c} \cdot \frac{\partial M^\pm}{\partial s} \tag{12}$$

$$0 = -\int_1^2 (P_n \cdot \cos\theta - P_t \cdot \sin\theta) r \cdot ds + \left\{r \cdot \left[\bar{\tau} + k_c\left(c_\phi^2 - c_m^2\right) + c_\phi M_\pm\right]\sin\theta - r \cdot \left[2k_c\frac{\partial \bar{c}}{\partial s} + \frac{\partial M_\pm}{\partial s}\right]\cos\theta\right\}_1^2 \tag{13}$$

$$2\bar{\sigma}_s \cdot h = \frac{\partial M_\pm}{\partial s} \tag{14}$$

where the planar tension and monolayer bending energies combine to define a new scalar field $\bar{\tau}$.

Since the interior of the bilayer is fluid and the layers are not chemically bonded, there is no static coupling stress ($\bar{\sigma}_s = 0$) at the interface between monolayers. Therefore, the difference in planar tension fields between monolayers is uniform (constant) over the surface. In the particular case where bilayers are merely pressurized by uniform hydrostatic pressure P, Eqs. (11–14) reduce to a single expression that describes the surface shape,

$$\frac{f_z}{2\pi} = -\left(\frac{p \cdot r^2}{2}\right) + \left\{r \cdot \left[\bar{\tau} + k_c\left(c_\phi^2 - c_m^2\right) + c_\phi M_\pm\right]\sin\theta - 2k_c r \cdot \frac{\partial \bar{c}}{\partial s} \cdot \cos\theta\right\} \tag{15}$$

Here, f_z, P, $\bar{\tau}$, $M\pm$ are invariants (constants) of the shape conjugate to extensive geometric parameters: i.e., axial length, interior volume and monolayer areas. For suspended capsules ($f_z = 0$),

Eq. (15) becomes equivalent to Euler-Lagrange relations derived by Helfrich and others [5,6,13,14] through minimization of membrane energy with respect shape variations. As established previously [14,17], elastic energy of a bilayer can be modeled by superposition of a local term for bending,

$$k_c \int\int \bar{c}^2 \cdot dA$$

plus two stretch energy terms that — for fluid monolayers — are uniform over the surface (global in character),

$$\frac{K}{A_o}\left\{\left(\int\int dA - A_o\right)^2 + \frac{1}{2}\left(\frac{h}{a}\int\int \bar{c}\cdot dA - \Delta A_o\right)^2\right\}$$

The first term in the stretch energy is produced by mean dilation of the monolayers in a bilayer as characterized by a uniform tension,

$$\bar{\tau} = 2K\left(\int\int dA - A_o\right)/A_o$$

The second term results from differential dilation between monolayers and leads to a uniform tension couple specified by,

$$M_{\pm} = \left(\frac{Kh}{a}\right)\left(\frac{h}{a}\int\int \bar{c}\cdot dA - \Delta A_o\right)$$
$$\equiv \bar{k}_c\left(\int\int \bar{c}\cdot dA - a\cdot\Delta A_o/h\right)$$

where the relative area expansion is given by,

$$\Delta A = \frac{h}{a}\int\int \bar{c}\cdot dA$$

ΔA_o is the initial area difference between monolayers established by history of vesicle formation and chemical composition. Therefore, the elastic Hamiltonian is the sum of a local bending energy, a global dilation energy, and a global bending energy in the following form:

$$E = k_c \int\int \bar{c}^2\cdot dA + \frac{\bar{\tau}}{2}\left(\int\int dA - A_o\right)$$
$$+ \frac{M_{\pm}}{2}\left(\int\int \bar{c}\cdot dA - a\cdot\Delta A_o/h\right) \qquad (16)$$

This relation defines zero-temperature shapes of bilayer capsules [14] and can be used to predict collective excursions from these shapes driven by thermal excitation at nonzero temperatures [16]. The relatively succint equations for bilayer shape (Eq. 15) and elastic energy (Eq. 16) are peculiar to quiescent bilayers. As we will see next, the situation for dynamic bilayers is considerably more complex.

4. Fluid bilayers: dynamics

4.1. Surface and environmental fluid dissipations

The bilayer and environment impede response to applied forces through viscous dissipation from three principal sources: hydrodynamic movements of water, mean surface convection of the bilayer, and differential (sliding) flow between monolayers. Constitutive descriptions for the first two contributions are given by classical proportionalities of stresses to gradients of velocity well known for Newtonian fluids. Since we can neglect fluid inertia, divergence of the stress field is sufficient to establish equations of motion for the environmental (aqueous) fluid as specified by,

$$\vec{\nabla} P = \eta_w \nabla^2 \vec{v}$$
$$\vec{\nabla}\cdot\vec{v} = 0 \qquad (17)$$

where P is the hydrostatic pressure field conjugate to the incompressibility requirement ($\vec{\nabla}\cdot\vec{v} = 0$ that maintains constant fluid density. (Although these 'creeping flow' equations appear simple, the solution for the velocity field v is often difficult to obtain.) The important consequence for the bilayer is the traction applied to the surface through the normal and tangential stress components of the hydrodynamic flow as symbolized by,

$$\sigma_n = -p + 2\eta_w \frac{\partial v_s}{\partial x_n}$$

$$\sigma_s = \eta_w\left(\frac{\partial v_s}{\partial x_n} + \frac{\partial v_n}{\partial x_t}\right)$$

where x_n, x_t are coordinates local to the membrane surface along normal and tangent directions, respectively; v_n and v_t are local components of velocity appropriate to these coordinates.

As in the bulk fluid, viscous dissipation is produced in coherent flow of the bilayer as a 'unit' surface. This convection of surface can be viewed as superposition of shear and dilational flows. Dilatation of the bilayer is always extremely small so the surface flow can be approximated as incompressible, which allows membrane stresses to be modeled by 2-D Newtonian relations,

$$\mathring{\tau}_m = \mathring{\tau} + 2(\eta_l \cdot h)V_s$$
$$\mathring{\tau}_\phi = \mathring{\tau} - 2(\eta_l \cdot h)V_s \tag{18}$$

The 'surface-isotropic' tension $\mathring{\tau}$ is a 2-D hydrostatic stress and V_s is the surface rate of shear. Here, surface viscosity ($\eta_l h$) is represented by an *apparent* 3-D coefficient of viscosity η_l multiplied by thickness as if the bilayer were a homogeneous liquid film. (In general, the dynamic stresses produced by viscous dissipation within the monolayer structure will be non-uniform along the chains and lead to dynamic moments. However, we will neglect these moments since the mean surface flow stresses are themselves very small as a consequence of the implicit dependence on thickness in the surface viscosity.) When contributions from viscous surface flow are added to the tension fields in Eqs. (11), (12) or (13), the force balances for a stationary surface can be extended to describe a moving bilayer in the 'creeping flow' limit simply by introducing the following terms:

$$\cdots + 2(\eta_l h)V_s(c_m - c_\phi) \tag{11}$$

$$\cdots + 2(\eta_l h)\left\{\frac{\partial V_s}{\partial s} + \frac{2V_s}{r}\cdot\frac{\partial r}{\partial s}\right\} \tag{12}$$

$$\cdots + 2(\eta_l h)\{r \cdot V_s \cdot \sin\theta\}_1^2 \tag{13}$$

Comparing these terms to the hydrodynamic stresses imparted on the bilayer by movement through the aqueous environment, we see that there is a crossover length $\delta_\otimes \sim \eta_e \cdot h/\eta_w$ above which dissipation in the aqueous environment is expected to dominate over viscous losses due to bilayer surface convection [17]. For typical lipid bilayers, this length is of order 100 h (~ 0.1 μm) or less [18,19].

To complete the equations of motion for the moving bilayer, the rate of surface shear V_s must be defined in terms of the velocity components v_s, v_n of material points on the surface. Based on the kinematics of displacements for arcs along meridian contours and tangent to latitude circles of the moving shape, rates of deformation can be related to components of velocity through the following equations:

$$V_m = \frac{\partial v_s}{\partial s} + c_m \cdot v_n$$
$$V_\phi = \frac{v_s}{r}\cdot\frac{\partial r}{\partial s} + c_\phi \cdot v_n \tag{19}$$

where the lead terms account for flow over a fixed axisymmetric shape and the latter terms result from the changes of dimensions as the surface moves outward along the normal. From these principal rates of deformation, rates of dilatation V_α and surface shear V_s are found to be,

$$V_\alpha \equiv V_m + V_\phi = \frac{1}{r}\frac{\partial}{\partial s}(r \cdot v_s) + \bar{c} \cdot v_n$$
$$V_s \equiv (V_m - V_\phi)/2$$
$$= \frac{1}{2}\left\{r\frac{\partial}{\partial s}(v_s/r) + (c_m - c_\phi)v_n\right\} \tag{20}$$

Thus, incompressible surface flow is specified by $V_\alpha = 0$. As we will discuss next, even though surface flow is nearly incompressible, the small compressibility of monolayers enables small differences in density to arise that promote important and unexpected relative motion. Because the difference in velocity between layers is usually small by comparison to mean surface convection, the tangential component v_t of velocity in the aqueous environment adjacent to the bilayer can be approximated by the mean velocity of the surface (i.e., $v_t \cong v_s$). (Note: for situations where the shape remains nearly constant ($v_n \sim 0$), the bilayer moves tangent to the surface and incompressibility ($V_\alpha = 0$) yields a simple spatial form for the flow field, i.e., $v_s \sim 1/r$.)

4.2. Interlayer dissipation

Because of the proportionality to thickness, mean surface flow stresses in bilayers are usually small. However, by comparison, the interfacial drag between monolayers can be enormous if the

relative velocity $v_s^{\pm} = v_s(2) - v_s(1)$ becomes significant since this viscous stress scales as the reciprocal of thickness, i.e.,

$$\bar{\sigma}_s = \frac{\eta_l}{x_s} \cdot v_s^{\pm} \equiv b \cdot v_s^{\pm}$$

where x_s ($< h$) is the thickness scale for momentum exchange at the interface between monolayers. Phenomenologically, interlayer dissipation is modeled properly by a viscous drag coefficient b ($= \eta_l / x_s$) since momentum transport occurs over distances well-below the continuum scale for hydrodynamics. As such, the drag coefficient will be sensitive to local molecular structure and motions at the monolayer 'brush polymer' interface. Examining differences between monolayer tension fields caused by interlayer drag (Eq. 9), we find that the relative velocity between fluid layers couples directly to the differential density (dilation) field $\alpha_{\pm}$, i.e.,

$$v_s^{\pm} = \left(\frac{K}{2b}\right) \frac{\partial \alpha_{\pm}}{\partial s} \tag{21}$$

(*Note:* a small contribution $[1/r(\eta_e h/b)\{V_s(2) - V_s(1)\}\partial r \partial s]$ from conventional viscous stresses in the surface is $\sim O(h^2)$ and can be neglected.) Consequently, drag at the monolayer-monolayer interface leads to nonuniform differences in density between layers. Likewise, nonuniform elastic dilation of one layer in excess of the other is opposed by viscous drag at the interface. Fig. 3 shows an idealized metaphor for this behavior based on a conceptual 'bilayer' film balance with independent monolayer sweeps and separate tension measurements. When a step difference of tension is applied in this film balance, the instantaneous response is impeded by the interlayer drag so that the area difference builds up gradually. However, at long times, the layers slide past one another to reach equilibrium with different uniform areas and tensions.

The dynamic change in differential density is given precisely by the difference in local rates of dilation between layers. Extending kinematics of flow to include surfaces separated by $\pm h/a$ from the mid surface, we find that dynamic changes in differential density between layers are given by divergence of the differential velocity field $v_s^{\pm}$ over the surface plus local dynamic changes in curvature, i.e.,

$$\frac{d\alpha_{\pm}}{dt} = \frac{1}{r}\frac{\partial}{\partial s}(r \cdot v_s^{\pm}) + \left(\frac{2h}{a}\right) \cdot \frac{d\bar{c}}{dt} \tag{22}$$

(*Note:* $d(...)/dt$ includes both changes in time observed from a fixed spatial reference and convected changes, $d(0...)/dt = \partial(...)/\partial t + v_s \partial(...)/\partial s$.) From Eqs. (21) and (22), we establish the conservation equation that describes dynamic evolution of the differential density field:

$$\frac{d\alpha_{\pm}}{dt} = D \cdot \nabla_s^2 \alpha_{\pm} + \left(\frac{2h}{a}\right) \cdot \frac{d\bar{c}}{dt}$$

where $\nabla_s^2(...)$ is the surface Laplacian operator defined by $1/r\ \partial[r \cdot \partial(...)/\partial s]/\partial s$. Surprisingly, nonuniformities in differential density relax by a nonlocal diffusion-like process over the surface and are stimulated by either rapid local changes in curvature or convection of bilayer between regions of high and low curvature. The apparent 'diffusivity' D represents dissipation of elastic energy through viscous drag at the monolayer-monolayer interface (illustrated by the conceptual metaphor in Fig. 3). In real situations, the differ-

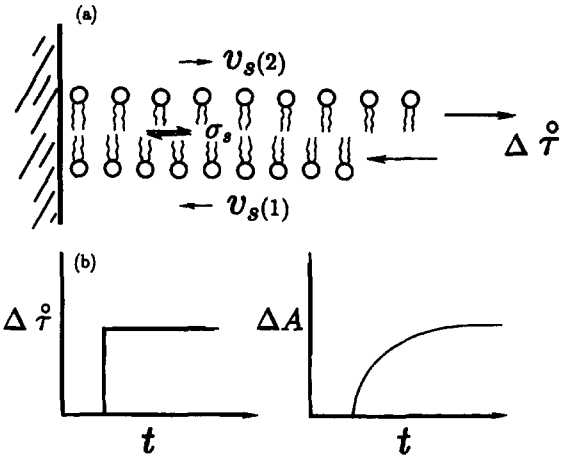

Fig. 3. (A) Sketch of a hypothetical bilayer 'film balance' where separate sweeps apply different tensions to the monolayers in order to expose dynamic opposition to interlayer density differences. (B) Left: a step difference between monolayer tensions is applied to the bilayer. Right: the area difference between layers initially grows steadily but eventually slows to approach equilibrium where a uniform difference in density exists between monolayers.

ential density can also relax by exchange or permeation of molecules through the interface from one layer to the other ('flip-flop'). Phenomenologically, such an effect can be modeled by a flux proportional to the field and regulated by a rate constant $1/t_p$. Including this relaxation mechanism (which is considered to be extremely slow in lipid bilayers), the full conservation equation for the differential density field becomes,

$$\frac{d\alpha_\pm}{dt} = D\cdot\nabla_s^2\alpha_\pm + \left(\frac{2h}{a}\right)\cdot\frac{d\bar{c}}{dt} - \alpha_\pm/t_p \qquad (23)$$

In turn, multiplication by the factor $(a\cdot\bar{k}_c/h)$ exposes the time-dependent behavior of force coupling between monolayers in the bilayer,

$$\frac{dM_\pm}{dt} = D\cdot\nabla_s^2 M_\pm + 2\bar{k}_c\cdot\frac{d\bar{c}}{dt} - M_\pm/t_p \qquad (24)$$

When combined with Eqs. (11), (12) or (13), including viscous surface stresses, Eq. (24) completes the set of relations required to predict the time-dependent response of a lipid bilayer to external forces. We see that the dynamic coupling field $M_\pm$ acts through curvature to impede the response of shape to external fields. Consequently, this hidden dynamic field should be important in bending excitations, geometric phase transitions, protrusion of small highly-curved regions from large vesicles, etc. To demonstrate the nonlocal features of layer coupling and the strong dynamic impedance to rapid changes in curvature, we will apply these equations to analysis of steady formation of a bilayer tether from a macroscopic-size vesicle.

5. Extraction of a submicroscopic tube from a cell-size vesicle

Tether formation from cell-size capsules is a ubiquitous phenomenon. For example, when a vesicle sticks to a foreign surface at a point and is then pulled away, an optically-invisible bilayer tube (diameter $<$ 100 nm) connects the vesicle to the surface even when the two become separated by many vesicle diameters. Likewise, when vesicles are dehydrated to create large excesses of surface area, spherical-like 'blebs' appear that are appended to the vesicles by invisible tubes of bilayer. Indeed, following initial hydration of lipid lamelli with excess water, many of the vesicles in a dispersion remain interconnected by tethers that are essentially *umbilical* remnants of attachments to the *maternal* lipid layers. Formation of tethers is also routinely H observed from cells and may have important biological function. The plethora of tether phenomena demonstrate that it is extremely difficult to disrupt the closed-spherical topology preferred by lamellar-phase lipids. Two physical conditions are requisite for tether formation, i.e., localization of force to a spot on the surface and existence of excess area in the capsule (above that sufficient to enclose the volume by a sphere). The key feature is that membrane is forced to flow between regions of enormously different curvature, e.g., from 10^5 m^{-1} to 10^8 m^{-1}! This creates a major source for the dynamic coupling field $M_\pm$ in Eq (24) and relative motion between layers.

5.1. Controlled tether formation

To demonstrate the dynamics of tether formation, we analyze a model situation (recently achieved experimentally [16]) where a slightly dehydrated vesicle is first pressurized into spherical form by micropipet suction as shown in Fig. 4. The projection of bilayer inside the pipet provides a reservoir of material that allows tether formation. Second, a small solid bead is touched to the bilayer at the pole opposite to the pipet entrance where a strong point attachment is made by some adhesive mechanism. When the pipet holding the vesicle is withdrawn, a tether is formed as demonstrated in Fig. 4. Assuming that the bead is bonded to a stationary force transducer, the axial force f_z can be measured as a function of rate of tether extraction. The model design has two important auxiliary features: (i) pipet suction sets the level of tension in the vesicle bilayer, which we will show tunes the tether diameter; and (ii) observation of change in projection length ΔL_p inside the pipet as tether length ΔL_t changes provides macroscopic measurement of the *invisible* tether diameter $2\cdot r_t$, i.e., $r_t \sim R_p\,(dL_p/dL_t)$ where $2\cdot R_p$ is the pipet caliber. (*Note:* a similar type of experiment has been developed [21] using gravitational

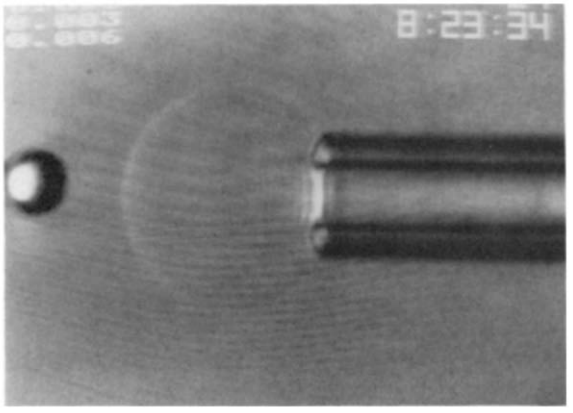

Fig. 4. Video micrograph of a slightly-dehydrated lipid bilayer vesicle (diameter ~ 20 μm) pressurized to a spherical form by micropipet aspiration. The solid microbead at the left is connected to the vesicle by an optically-invisible tube of bilayer (a tether of ~ 40 nm diameter). The tether formed following point adhesion of the bead to the vesicle surface by ligands to receptor-conjugated lipids (see [16] for details).

force to pull on the attached bead. This is somewhat more complicated since the falling bead leads to a variable hydrodynamic force [15].) Our objective is to examine the dependence of tether force on extraction rate and to compare the impedance to flow from conventional fluid dissipations with that from intermonolayer drag. To simplify analysis, we will first determine the tether force neglecting interlayer dissipation and then consider the situation where interlayer drag is dominant. Based on experimental results, we will demonstrate that interlayer drag slows the speed of tether formation about 20-fold below that expected for conventional fluid retardation!

5.2. *Conventional hydrodynamic forces*

Beginning with hydrodynamic dissipations, withdrawal of the pipet produces drag on the vesicle from movement through the aqueous environment; this is predicted by low Reynolds-number flow relations for an incompressible fluid as noted earlier. Assuming that the tension in the vesicle surface is sufficiently large, the shape will remain closely spherical (which is verified experimentally). Thus, we approximate the drag on the vesicle by the shear stress for Stokes' flow past a sphere [22], i.e.,

$$P_t \approx -(3\eta_w/2R)\dot{L}_t \cdot \sin\theta$$

The tether is stationary once formed so there is no significant drag on its surface from water flow. Furthermore, there is a small aqueous circulation inside the vesicle (and into the tether) driven by bilayer surface flow that can also be shown to offer negligible resistance to formation of a submicroscopic tether. However, dissipation in surface flow of the bilayer is not neglible. Because of the stiff-condensed state of the bilayer, surface convection can be approximated by incompressible surface flow over the fixed shape that is given by $v_s = -\dot{L}_t(r_t/r)$ starting at the vesicle-tether junction where the radius and velocity are r_t and $-\dot{L}_t$. Introducing the surface flow H field and aqueous shear stress into Eq. (14) (modified for dynamic surface stresses), the gradient in meridional tension τ_m $(\approx)\bar{\tau} + 2\eta_l h \cdot V_s$) due to hydrodynamic effects is predicted over the vesicle surface, i.e.,

$$\left(\frac{3\eta_w \dot{L}_t}{2R}\right)\sin\theta \approx \frac{\partial \tau_m}{\partial s} + \frac{1}{r^3}\left(4\eta_l h r_t \dot{L}_t\right)\cos^2\theta$$

(*Note:* bending contributions to the tension field can be neglected over the large vesicle (radius $R \gg r_t$) because they scale as $k_c/R^2\bar{\tau}$. Typically, this ratio is significantly below 10^{-3} for 10-μm vesicles and tensions $> 10^{-3}$ mN/m.) When integrated from the vesicle-tether junction to distances much larger than the tether radius, the last term gives a tension increase at the tether due to bilayer dissipation [$\sim (2\eta_l h/r_t)\dot{L}_t$]. On the other hand, integration of the aqueous drag over the whole vesicle gives a tension reduction at the tether [$\sim -3\eta_w \dot{L}_t$]. Including the level of tension set by pipet suction P_p, i.e., $\tau_m(p) \approx P_p R_p/2(1 - R_p/R)$, the force supported by the tether is calculated simply from Eq. (15) as,

$$f_z \approx 2\pi[r_t \cdot \tau_m(p) + k_c/r_t] + 2\pi[2(\eta_l h) - 3(\eta_w r_t)]\dot{L}_t \qquad (25)$$

The hydrostatic pressure force can be neglected inside the extremely small tube. Because the

tether radius is small, bending stiffness *does* contribute to the axial force. As will be discussed in detail later, bending stiffness plays a dominant role in stabilizing the radius of the tether. More at issue now is the dynamic force, which is linearly proportional to velocity for inertialess flows as expected. Also not surprising, the crossover length between surface and aqueous hydrodynamic losses shows up explicitly in the ratio of the two terms in the velocity coefficient, i.e., $r_t \sim \delta_\otimes = \eta_l h/\eta_w \sim 0.3\ \mu m$. Interestingly, when the vesicle is pulled through the aqueous fluid, the Stokes' drag acts to diminish the dissipation in bilayer surface flow — the work being supplied externally by translation of the pipet. However, if the vesicle is forced to move by flowing fluid past the body, the sign of the drag would change and the tether force would increase in proportion to relative velocity of the external flow.

5.3. A hidden dynamic force

Now, we neglect conventional hydrodynamics and examine the effect of interlayer coupling through evolution of the tension couple $M_\pm$. For steady convection of the bilayer surface over the fixed shape, the conservation equation for the interlayer coupling (Eq. 24) reduces to,

$$\frac{\partial M_\pm}{\partial t} = \frac{D}{r}\frac{\partial}{\partial s}\left\{r\cdot\frac{\partial M_\pm}{\partial s} + P_e\cdot\left(M_\pm - 2\bar{k}_c\cdot\bar{c}\right)\right\}$$

where convective contributions are scaled by a dimensionless ratio $Pe = r_t\dot{L}_t/D$ of surface convection (flux) to diffusivity called the Peclet number in other contexts [22]. (*Note:* relaxation of the coupling field by interlayer exchange — 'flip-flop' — is neglected here because of the tether is assumed to be formed rapidly.) Even when bilayer tethers are pulled at enormous rates of hundreds of $\mu m/s$, the ratio of diffusivity to surface flux $(1/Pe)$ exceeds 10^3. Therefore, in tether formation, convection of the coupling field will be negligible in comparison to diffusion. Gradients in the field will spread quickly beyond the source region at the tether junction. Consequently, the explicit time derivative $\partial M_\pm/\partial t$ will be well approximated by the surface divergence of the gradient field, which gives classical diffusion of the field driven by a steady flux at the site of the tether, i.e.,

$$\frac{\partial M_\pm}{\partial t} \approx D\cdot\nabla_s^2 M_\pm$$

$$D\cdot\frac{\partial M_\pm}{\partial s}\Big|_{r_t} = 2\bar{k}_c\,\dot{L}_t$$

The local flux of differential density arises from bilayer flow through the sharp change in curvature at the vesicle-tether junction. From a kinematic perspective (illustrated in Fig. 5), the diffusive flux is produced by rapid relative flow between monolayers; this is required to conserve mass in transport to the tether: i.e., mass flux to the outer surface of the tether exceeds mass flux to the inner surface. The relative velocity between layers is scaled by $\dot{L}_t h/r_t$, which shows that molecules in opposite layers slide past at rates of order $\dot{L}_t/r_t$ as they approach the tether. Analytically, the situation is exactly analogous to diffusion of *temperature* (the coupling field $M_\pm$) over a cold sphere driven by local *heating* (the rapid change in curvature) at one pole. For steady eating, the process is quickly dominated by the slowest component in a Fourier time series so that a simple convolution approximation can be used to evaluate the effective field near the source [16]. As such, nonlocal gradients of temperature arise along with increase in average temperature as

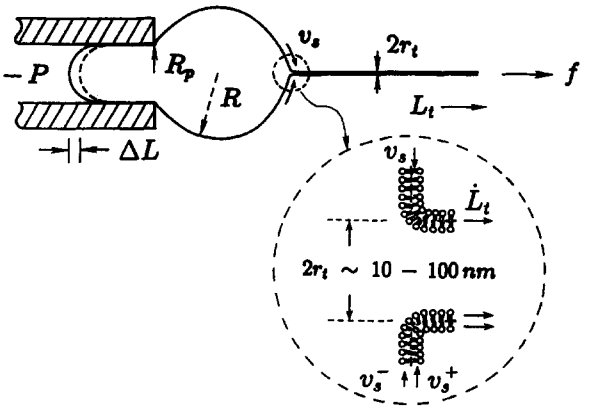

Fig. 5. Kinematic illustration of the relative flow produced between layers as the bilayer is forced to flow through a region of enormous change in curvature (~ 1000-fold increase) as it forms an ultrasmall tube.

time progresses because the surface is closed. Carrying this analysis over to tether extraction at constant rate, the tension couple applied to the tether can be shown to include two contributions — one proportional to rate of tether formation and the other proportional to tether length — given by,

$$M_{\pm} \approx b \cdot h^2 \ln(R/r_t)\dot{L}_t + \left(\frac{\bar{k}_c}{2R^2}\right) L_t \qquad (26)$$

Consistent with 2-D diffusion, the dynamic coefficient in the force depends weakly (logarithmically) on vesicle and tether dimensions. The remaining task is to evaluate the tether force and show that the tether is a uniform cylinder.

As in the hydrodynamic analysis, the axial force applied by the vesicle to the tether is specified by Eq. (15) — the difference in this case being a contribution from the interlayer coupling field as follows:

$$f_z \approx 2\pi\left(r_t \cdot \bar{\tau} + \frac{k_c}{r_t} + M_{\pm}\right) \qquad (27)$$

Eq. (27) immediately exposes the impact of interlayer coupling on tether force; but before discussion, two aspects of the process must be considered. First, it is apparent from Eq. (12) that addition of dynamic coupling between layers contributes to gradients in the tension field, i.e.,

$$\frac{\partial \bar{\tau}}{\partial s} = -\bar{c} \cdot \frac{\partial M_{\pm}}{\partial s}$$

Clearly, over the macroscopic vesicle surface, the extremely small curvature eliminates the contribution of the coupling field so that tension is essentially uniform and equal to $\tau_m(p)$ set by pipet suction. Furthermore, because of rapid diffusion, the change in the coupling field through the submicroscopic region proximal to the tether can also be neglected. Hence, we can accept that the tension field at the tether junction is established by mechanical pressurization of the vesicle.

Next, another mechanical feature can be exploited that accompanies external regulation of tension: i.e., control of tether diameter. This follows directly from Eq. (11) for the balance of forces along the normal to the tether surface:

$$r_t p \approx \bar{\tau} - k_c/r_t^2$$

Again, the coupling field is eliminated by the nearly-zero longitudinal curvature of the tether. Likewise, the action of hydrostatic pressure P is also eliminated through scaling with tether dimension. The important conclusion is that tether cross section is inversely related to tension, i.e., $r_t^2 = k_c/\tau_m(p)$, through bending rigidity [15,16]. If there is no gradient in tension due to hydrodynamic effects, vesicle tension uniquely determines the size of the *invisible* tube. To demonstrate that this surprising feature is in fact true, Fig. 6 presents measurements taken from tether extraction experiments. In Fig. 6A, for constant pipet suction, vesicle projection length L_p inside the pipet (the membrane reservoir) is observed to decrease linearly with increase in tether length L_t over hundreds of μm, which verifies that the tether radius is constant. In Fig. 6B, at different pipet suctions, the square of the tether radius is found to increase as the reciprocal of tension (*independent* of extraction rate), which verifies that tether diameter is set by vesicle pressurization. (*Note:* this approach provides a useful technique to measure the extremely small bending rigidity of lipid bilayers.)

With specification of tether cross section by mechanical tension, the tether force (Eq. 27) is reduced to a sum of an experimentally-controlled threshold (in existence before dynamic extraction),

$$4\pi\sqrt{k_c \cdot \tau_m(p)}$$

plus an excess force derived totally from tether growth. The excess force is given exactly by the interlayer coupling field at the tether junction (Eq. 26),

$$f_z = 4\pi\sqrt{k_c \cdot \tau_m(p)} + 2\pi\left[b \cdot h^2 \ln(R/r_t)\dot{L}_t + \left(\frac{\bar{k}_c}{2R^2}\right) L_t\right] \qquad (28)$$

We see that the tether force involves a dynamic (velocity-dependent) part driven by viscous drag at the monolayer-monolayer interface *and* a static (length-dependent) part that persists after tran-

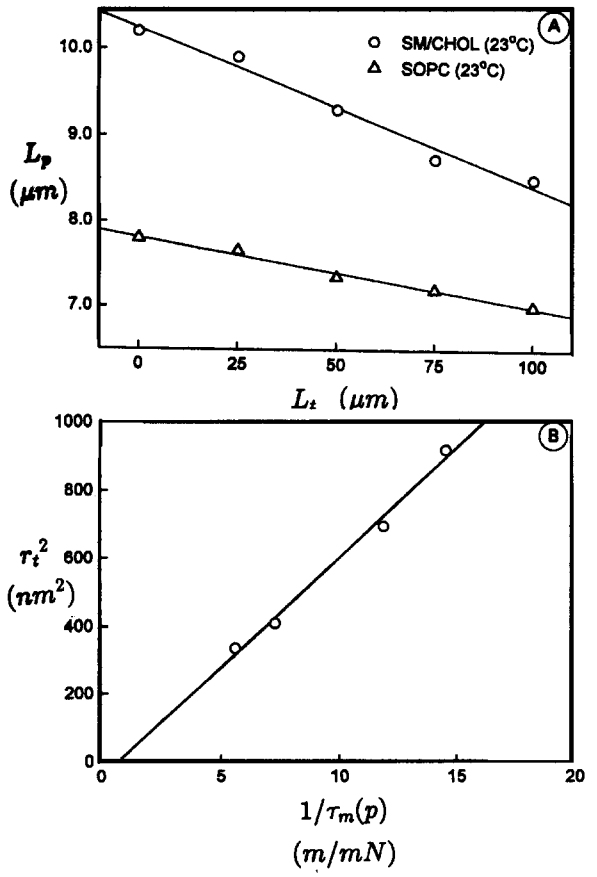

Fig. 6. (A) Measurements of vesicle bilayer projection L_p inside a pipet taken as length L_t of a tether was increased at uniform rate. Pipet suctions in these tests were held fixed to maintain constant tension (~ 0.09 mN/m) in the vesicle bilayers. The data were taken from tests of two vesicles with different lipid compositions: an equal mixture of sphingomyelin to cholesterol 1:1 and pure stearoyl oleoyl phosphatidyl choline. (*Note:* the linear behavior demonstrates that the tether radii (averaged over μm distances) were constant in both extraction tests.) (Data taken from [16]). (B) Taken from measurements of bilayer projection length versus tether length as shown in (A), the data for tether cross section (r_t^2) have been plotted as a function of reciprocal tension ($1\tau_m$) set by pipet suction. The slope of the linear proportionality yields the intrinsic elastic modulus k_c for bending monolayers of the bilayer. (*Note:* the elastic proportionality was found to be independent of tether velocity [16].)

sients in the coupling field have diffused away. Both forces are nonlocal consequences — elastic *and* dynamic — of coupling between monolayers in bilayers! Clearly, elasticity (force ~ length) of the tether comes from a global difference in area between monolayers, $\alpha_\pm \sim L_t h/R^2$, whereas, viscous response (force ~ velocity) to tether formation comes from diffusive spread, $\dot{L}_t h$, of relative density over the macroscopic surface. For tethers pulled from lipid vesicles, the nonlocal elastic force is very small (~ 10^{-12} N for a 100 μm tether) — the threshold force is somewhat greater (~ 10^{-11} N for a mechanical tension of 0.1 mN/m) — but the dynamic resistance can be much larger as we will show next. (*Note:* to illustrate magnitude of force, a *single* hydrogen bond is expected to break between forces of 10^{-10} and 10^{-11} N!).

5.4. Interlayer drag dominates resistance to tether flow

Since dynamic contributions to tether force are all linear in tether velocity, ratios of the coefficients in the dynamic forces predicted by Eqs. (25) and (28) expose important physical parameters for bilayer shape dynamics. First, we see that the comparison of impedance due to interlayer drag with viscous resistance from forced bilayer convection defines a ratio $b \cdot h \cdot \ln(R/r_t):2\eta_l$ or equivalently ~ $3h:x_s$ (noting that the logarithm is always of order 5–6 in experimental situations). Thus, the significance of interlayer dissipation in relation to dissipation in surface convection scales as the ratio of bilayer thickness h to the penetration depth x_s for momentum exchange at the monolayer-monolayer interface. Second, comparison of interlayer dissipation to dissipation in aqueous flow yields a product of two length ratios, i.e., $(h:x_s)\,(\sigma_\otimes:r_t)/2$, where $\sigma_\otimes$ is the length defined previously for cross over between surface and hydrodynamic flow dissipations. Since the tether radius is so small, it is apparent that interlayer drag overwhelms the force contributed to the tether by aqueous drag on the vesicle. More importantly, the comparison defines a crossover length $R_\otimes \sim \delta_\otimes h/x_s$ for radii of curvature below which interlayer dissipation dominates the dynamics of shape changes. Clearly, both dynamic cross overs depend on the distance scale for momentum exchange (dynamic coupling) between monolayers of the bilayer. This transport of momentum is expected to occur over distances less

than the bilayer thickness ($x_s < h$) because the hydrocarbon chains have less freedom for relative lateral motion away from the midplane (as shown by increased orientational ordering toward the hydrophilic surfaces [19,23]). Hence, interlayer dissipation is expected to produce a much larger dynamic resistance to tether growth than conventional flow dissipations — but how much larger?

From measurements of lateral mobility of probes (many of them attached to similar lipids) embedded in the surface, we know values of surface viscosity with sufficient certainty to calculate the impedance to tether flow produced by bilayer surface convection. For phosphatidyl choline PC lipids, surface viscosities of fluid phase bilayers lie in the range of 10^{-7} to 10^{-6} surface poise (or 10^{-10} to 10^{-9} N-s/m^2), which implies that the equivalent film viscosity η_l is of order 1 poise (0.1 N-s/m^2) for a thickness of ~ 3 nm [19,24]. Thus, we can anticipate the magnitude of dynamic force required to extract tethers from vesicles opposed only by viscous flow resistance of the bilayer, i.e., in Newtons $f \approx (10^{-9} - 10^{-8}) \times \dot{L}_t$ given $\dot{L}_t$ in m/s. Since the fastest rates of extraction in experiments are about 3–4 $\times$ 10^{-4} m/s (~ ten vesicle diameters in a second!), we see that conventional viscous dissipation in bilayer flow can only lead to miniscule tether forces of order 10^{-12} N. (*Note:* coincidentally, the *apparent* surface viscosity represented by $\eta_w r_t$ in Eq. (25) that scales aqueous flow resistance is of comparable order to $\eta_l h$ for the bilayer since tether radii are typically 2–4 $\times$ 10^{-8} m. So, if anything, the tether force produced by conventional flow resistances will be smaller.) However, much larger dynamic forces (2–3 $\times$ the threshold of 10^{-11} N) are required to pull tubes of PC bilayers from vesicles at these speeds as illustrated by the sample data plotted in Fig. 7 (taken from [16]). Astonishingly, the dynamic forces measured in these experiments were 20–30-times that expected for bilayer surface flow dissipation. Clearly, the dynamic force is driven by other mechanisms — the most obvious is interlayer drag as we have described.

Accepting that interlayer drag is the major source of dynamic impedance to tether formation, experimental correlation of force with rate of tether extraction provides a critical test of the

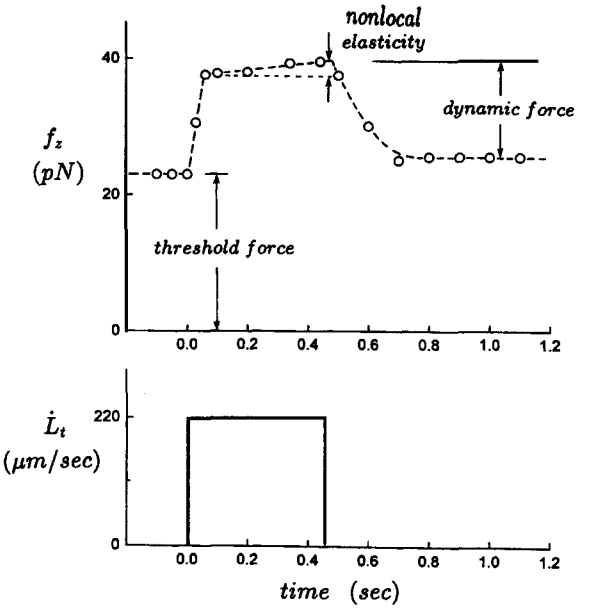

Fig. 7. Example of force response (top) produced by a brief step extraction of a tether at constant rate (bottom). Note: a threshold level of force exists prior to the dynamic extraction, which is set by tension (vesicle pressurization) and bilayer bending stiffness (as described in the text). Extraction at constant rate produces a small elastic force in the tether that increases slowly in time *plus* a large dynamic force that is proportional to the rate of extraction, both of which are consequences of nonlocal interlayer coupling in bilayer capsules.

postulated constitutive relation for interlayer coupling, i.e., $\bar{\sigma}_s = b \cdot v_s^{\pm}$.

As shown by the data for dynamic force plotted against tether velocity for PC bilayers in Fig. 8 (again taken from [16]), the linear coupling of interlayer shear stress to relative velocity is borne out by experimental evidence where the magnitude of coupling is embodied in a constant drag coefficient b (of order 10^8 N-s/m^3 for the data in Fig. 8). Importantly, tether extraction at these rates is equivalent to interlayer shear rates from 10^2 to 10^4 s^{-1} which, as mentioned before, represents the rate that molecules in opposite monolayers slip past each other as the bilayer approaches the tether. From the interlayer drag coefficient b, we can derive the *apparent* thickness scale x_s over which this intimate exchange of momentum takes place, i.e., $x_s \approx \eta_l/b$. Taking 0.1 poise as the characteristic viscosity for the

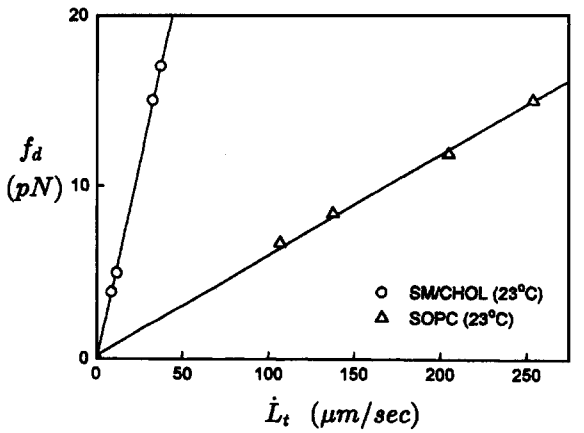

Fig. 8. Taken from measurements of force at different rates of extraction, dynamic tether forces f_d have been plotted as a function of tether velocity L_t for two types of vesicle bilayers. The linear proportionality of force to velocity yields a constant coefficient for interlayer drag, which clearly differs by almost an order of magnitude between the two types of bilayers.

hydrocarbon polymer core of the bilayer, we see that the thickness scale or depth of penetration for interlayer shear is of order 0.1 h based on this simple arithmetic, i.e., the value of x_s is about the dimension of a methylene group! Clearly, the deduction has little direct significance since this length represents molecular actions over distances well below continuum limits. However, the useful purpose is to demonstrate the exciting feature that this macroscopic measurement actually images molecular-scale interactions within the bilayer which were previously hidden from view. Hence, it is possible to study kinetic properties governed by motions normal to the bilayer and, moreover, governed by atomic scale dynamics at the monolayer-monolayer interface.

6. Summary

The objective here has been to emphasize important new physics of bilayers that comes about simply because the membrane is actually *two* weakly-adherent membranes which are restricted by a closed-spherical topology. Hopefully, we have successfully demonstrated that this obvious structural feature of bilayers leads to significant (but subtle) consequences in dynamics of curved bilayers throughout the mesoscale range of dimensions (< 1 μm). Finally, we perceive excellent opportunities to explore molecular determinants of lubricative interactions at well-defined interfaces between 'polymer brushes' (i.e., the hydrocarbon chains) and to expose relaxation processes internal to the bilayer driven by molecular transfer between layers ('flip-flop'). This will provide a unique experimental platform to evaluate molecular dynamics simulations and other microscopic theoretical predictions.

Acknowledgements

This work was supported by the Medical Research Council of Canada through grant MT 7477 and stimulated by involvement in the Canadian Institute for Advanced Research Program in 'Science of Soft Surfaces and Interfaces'.

Appendix: mechanical notes

A. Using the definitions for generalized tensions and moments given in Eq. (6) of the text, the force balances (Eqs. (2), (3) and (5)) for the equivalent surface can be rewritten in a form that is directly related to planar mechanical properties of membrane strata, i.e.,

$$p_n = \mathring{\tau}_m c_m + \mathring{\tau}_\phi c_\phi + (M_m + M_\phi) c_m c_\phi - \frac{1}{r}\frac{\partial}{\partial s}(rQ_m) \tag{2}$$

$$-P_t = \frac{1}{r}\frac{\partial}{\partial s}(r\cdot\mathring{\tau}_m) - \frac{\mathring{\tau}_\phi}{r}\cdot\frac{\partial r}{\partial s} + \bar{c}\cdot Q_m + (M_m - M_\phi)\frac{\partial c_\phi}{\partial s} \tag{3}$$

$$0 = -\int_1^2 (P_n\cdot\cos\theta - P_t\cdot\sin\theta) r\cdot ds + \left[r\cdot(\mathring{\tau}_m + c_\phi M_m)\cdot\sin\theta - r\cdot Q_m\cdot\cos\theta\right]_1^2 \tag{5}$$

B. As noted in the text, when forces are considered, material stresses in layers of a stratified membrane must be properly scaled by dimensions that are adjusted for deviations from the equivalent surface dimensions. Similarly, the external tractions P_n, P_t involve sums of the normal and

shear stresses σ_n, σ_s imparted to the bounding surfaces of the membrane,

$$P_n = \sigma_n^o(1 + h_o \cdot \bar{c}) - \sigma_n^i(1 - h_i \cdot \bar{c})$$

$$P_t = \sigma_s^o(1 + h_o \cdot \bar{c}) - \sigma_s^i(1 - h_i \cdot \bar{c})$$

where h_o, h_i account for location of the outer (o)/inner (i) surface areas relative to the equivalent mechanical surface. (*Note:* the positive sign convention implicit in the definition of shear stress is in the sense of the coordinate s on the outer surface but opposite to the direction of s at the inner surface of a stratum. Hence, positive shear stresses on both outside and inside of a membrane tend to cancel if they are of comparable magnitude (e.g., exterior hydrodynamic flows in opposite directions). However, shear stresses of opposite sign on the outer and inner surfaces act coincidentally to increase the total traction (e.g., exterior hydrodynamic flows in the same direction).)

C. Applying the balance of lateral forces defined by Eq. (7) to each layer of a bilayer and then taking the difference, we demonstrate that tension and moment differences between layers are coupled through intermonolayer drag as follows:

$$2\bar{\sigma}_s = \frac{1}{r}\frac{\partial}{\partial s}(r \cdot \Delta\mathring{\tau}_m) - \frac{\Delta\mathring{\tau}_\phi}{r} \cdot \frac{\partial r}{\partial s} + \bar{c}\left\{\frac{1}{r}\frac{\partial}{\partial s}(r \cdot \Delta M_m') - \frac{\Delta M_\phi'}{r}\frac{\partial r}{\partial s}\right\} + (\Delta M_m' - \Delta M_\phi')\frac{\partial c_\phi}{\partial s}$$

$$\Delta M_m' \equiv M_m(2) - M_m(1) + \frac{h}{a} \cdot \mathring{\tau}_m$$

$$\Delta M_\phi' \equiv M_\phi(2) - M_\phi(1) + \frac{h}{a} \cdot \mathring{\tau}_\phi$$

The contribution (i.e., $-\sigma_s^o(1 + h\,c/2) - \sigma_s^i(1 - h\,c/2)$) due to environmental shear stresses has been neglected since intermonolayer drag will be larger by a factor on the order of $\eta_l d_w/\eta_w x_s$. (η_l and η_w are coefficients of viscosity for the hydrocarbon core of the bilayer and water respectively; d_w and x_s are characteristic penetration depths of the velocity field into water and at the interface between monolayers, respectively.) In lipid bilayers, this ratio will always exceed 100 or so! For symmetric bilayers, the contribution to the equation above from the differences in moments $\Delta M_m'$, $\Delta M_\phi'$ is given by,

$$\bar{c}\left\{\frac{1}{r}\frac{\partial}{\partial s}(r \cdot \Delta M_m') - \frac{\Delta M_\phi'}{r}\frac{\partial r}{\partial s}\right\} + (\Delta M_m' - \Delta M_\phi')\frac{\partial c_\phi}{\partial s} \approx \frac{h}{a}\left\{-P_t \cdot \bar{c} + (\mathring{\tau}_m - \mathring{\tau}_\phi)\frac{\partial c_\phi}{\partial s}\right\}$$

This term is of higher order than gradients of the planar tension differences between layers so can be neglected. Consequently, differences in planar tension fields between layers of a bilayer are driven by the interlayer drag stress $\bar{\sigma}_s$ as expressed by Eq. (9) in the text.

References

[1] G.G. Shipley (1973) in: D. Chapman and D.F.H. Wallach (Eds.), Biological Membranes, Vol. II, Academic Press, New York, pp. 1–51.

[2] V. Luzzati, A. Gulik, T. Gulik-Krzywicki and A. Tardieu (1986) in: J.A.F. Op den Kamp, B. Roelofsen and K.W.A. Wirtz (Eds.), Lipids and Membranes: Past, Present and Future, Elsevier Science Publishers, Amsterdam, pp.137; V. Luzzati, P. Mariani and T. Gulik-Krzywicki (1987) in: J. Meunier, D. Langevin and N. Boccara (Eds.), Physics of Amphiphilic Layers, Springer Proceedings, Vol. 21, Springer-Verlag, Berlin, pp. 131–137.

[3] W. Helfrich (1973) Z. Naturforsch. 28c, 693–703.

[4] E. Evans (1974) Biophys. J. 14, 923–931.

[5] H.J. Deuling and W. Helfrich (1976) J. Phys. 37, 1335–1345.

[6] J.T. Jenkins (1977) J. Math. Biol. 4, 149–169.

[7] W. Helfrich (1978) Z. Naturforsch. 33a, 305–315; W. Helfrich and R.-M. Servuss (1984) Nuovo Cimento Soc. Ital. Fis D3, 137–151.

[8] M.B. Schneider, J.T. Jenkins and W.W. Webb (1984) J. Phys. 45, 1457–1472; S. Milner and S.A. Safran (1987) Phys. Rev. A 36, 4371–4379.

[9] E. Evans (1980) Biophys. J. 30, 265–284; E. Evans (1990) Colloids Surf. 43, 327–347.

[10] U. Seifert and R. Lipowsky (1990) Phys. Rev. A 42, 4768–4771.

[11] R. Lipowsky and S. Leibler (1986) Phys. Rev. Lett. 56, 2541–2544; R. Lipowsky and U. Seifert (1991) Mol. Cryst. Liq. Cryst. 202, 17.

[12] E. Evans and V.A. Parsegian (1986) Proc. Natl. Acad. Sci. USA 83, 7132; E. Evans (1991) Langmuir 7, 1900–1908.

[13] S. Svetina and B. Žekš (1989) Eur. Biophys. J. 17, 101–111; K. Berndl, J. Käs, R. Lipowsky, E. Sackmann and U. Seifert (1990) Europhys. Lett. 13, 659–664; U. Seifert, K. Berndl, R. Lipowsky (1991) Phys. Rev. A 44, 1182–1202.

[14] L. Miao, B. Fourcade, M. Rao, M. Wortis and R.K.P. Zia (1991) Phys. Rev. A 43, 6843–6856; L. Miao, U. Seifert, M. Wortis and H.-G. Döbereiner (1994) Phys. Rev. E49, 5389–5407.

[15] E. Evans, A. Yeung, R. Waugh and J. Song (1992) in: R. Lipowsky, D. Richter and K. Kremer (Eds.), The Structure and Conformation of Amphiphilic Membranes, Springer Proceedings Vol. 66, Springer-Verlag, Berlin, pp. 148–153.

[16] A. Yeung (1994) Ph.D. Thesis, Department of Physics, University of British Columbia, Canada.

[17] E. Evans and R. Skalak (1980) Mechanics and Thermodynamics of Biomembranes, CRC Press, Florida.

[18] E. Evans and D. Needham (1987) J. Phys. Chem. 91, 4219–4228.

[19] M. Bloom, E. Evans and O.G. Mouritsen (1991) Q. Rev. Biophys. 24, 293–397.

[20] E. Evans and W. Rawicz (1990) Phys. Rev. Lett. 64, 2094–2097.

[21] L. Bo and R.E. Waugh (1989) Biophys. J. 55, 509–517.

[22] L.D. Landau and E.M. Lifshitz (1982) Fluid Mechanics, Pergamon Press, New York.

[23] J. Seelig and A. Seelig (1980) Q. Rev. Biophys. 13, 19–61; M. Lafleur, P.R. Cullis, B. Fine and M. Bloom (1990) Biochemistry 29, 8325–8333.

[24] R. Merkel, E. Sackmann and E. Evans (1989) J. Phys. 50, 1535–1555; W.L.C. Vaz, Z.I. Derzko and K.A. Jacobson (1982) in: G. Poste and G.L. Nicolson (Eds.), Cell Surface Reviews, Vol. 8: Membrane Reconstitution, Elsevier, pp. 83–136.